applied sciences

MDPI

Article

Effects of C(2) Methylation on Thermal Behavior and Interionic Interactions in Imidazolium-Based Ionic Liquids with Highly Symmetric Anions

Boumediene Haddad [1,2,3], Johannes Kiefer [4,5,6,*], Houari Brahim [1], El-habib Belarbi [2], Didier Villemin [3], Serge Bresson [7], Ouissam Abbas [8], Mustapha Rahmouni [2], Annalisa Paolone [9] and Oriele Palumbo [9]

1 Department of Chemistry, Dr Moulay Tahar University of Saida, Saida 20000, Algeria; haddadboumediene@yahoo.com (B.H.); brahim.h@outlook.com (H.B.)
2 Synthesis and Catalysis Laboratory LSCT, Tiaret University, Tiaret 14000, Algeria; belarbi.hb@gmail.com (E.B.); m.rahmouni@mesrs.dz (M.R.)
3 Laboratoire de Chimie Moléculaire et Thio-organique, Ensicaen, Centre national de la recherche scientifique (CNRS), University of Caen, 14050 Caen, France; didier.villemin@ensicaen.fr
4 Technische Thermodynamik and MAPEX Center for Materials and Processes, Universität Bremen, 28359 Bremen, Germany
5 School of Engineering, University of Aberdeen, Aberdeen AB24 3UE, UK
6 Erlangen Graduate School in Advanced Optical Technologies (SAOT), Friedrich-Alexander-Universität Erlangen-Nürnberg, 91052 Erlangen, Germany
7 Laboratoire de Physique des Systèmes Complexes, Université Picardie Jules Verne, 80039 Amiens, France; sergebresson@yahoo.fr
8 Centre Walloon de Recherche Agronomique, CRA-W, Bâtiment Maurice Henseval, 50030 Gembloux, Belgium; o.abbas@cra.wallonie.be
9 Consiglio Nazionale delle Ricerche, Istituto dei Sistemi Complessi, Università degli Studi di Roma La Sapienza, 00185 Roma, Italy; annalisa.paolone@roma1.infn.it (A.P.); oriele.palumbo@roma1.infn.it (O.P.)
* Correspondence: jkiefer@uni-bremen.de; Tel.: +49-421-218-64777

Received: 8 June 2018; Accepted: 20 June 2018; Published: 26 June 2018

Featured Application: The study aims at making a step towards the rational design of ionic liquids for specific applications. The key to this rational design is to fully understand the structure-property relationships. In other words, knowing the links between the behavior at the molecular and the macroscopic scale will enable to develop materials/fluids with optimal properties for a given application, e.g., a chemical process or an electrochemical device.

Abstract: The chemical and physical properties of imidazolium-based ionic liquids are determined by the interactions between the counter-ions. The C(2) position plays an important role in these interactions, as it represents the predominant site for interionic hydrogen bonding. This study shows that the directional hydrogen bonds between highly symmetrical anions (iodide, tetrafluoroborate, hexafluorophosphate) and the C(2)-H group of the 1-methyl-3-propylimidazolium cation determine the molecular and macroscopic behavior in terms of the thermal properties. Upon replacing the C(2) proton by a methyl group, the anion repositions itself at the C(4)/(5) moiety, where it forms a new hydrogen bond, apparently with only one of the two CH groups. In addition, the larger the anion is in diameter, the more likely it will establish further interactions with other parts of the cation, such as the propyl chain.

Keywords: hydrogen bonding; ionic liquid; imidazolium; vibrational spectroscopy

1. Introduction

Ionic liquids (ILs) are typically composed of bulky organic cations and inorganic or organic anions. They represent fascinating materials in the liquid as well as the solid state, with numerous potential applications in electrochemistry and chemical engineering [1,2]. Interionic interactions between cations and anions are known to govern the molecular and macroscopic properties of 1,3-dialkylimidazolium–based ionic liquids. In particular, the C(2) position plays a crucial role in this respect, because the charge distribution in the aromatic ring leads to enhanced polarization and hence a slightly acidic nature of the C(2)-H bond. Consequently, the C(2) proton is the favorable hydrogen-bond donor. A comprehensive overview has recently been given by Pascoal et al. [3].

Most studies to date have focused on the interionic interactions of ionic liquids, in which the 1,3-dialkylimidazolium cation is combined with nonsymmetrical anions, exhibiting rather well-defined moieties for establishing hydrogen bonds. The list of investigated anions includes bis(trifluoromethylsulfonyl) imide [4–7], nitrate [8], alkyl sulfates [5,9], dicyanamide [5,10], thiocyanate [5], acetate [11,12], hydrogen sulfate [13,14], and trifluoromethanesulfate [15,16]. On the other hand, interactions with highly symmetrical anions have been studied less. Examples include the halogenides [17–19], tetrafluoroborate [20,21], and hexafluorophosphate [15,22]. However, systematic studies with varied anions are rare [23] or have had a different focus, e.g., on the rotational isomerism of the cation [24].

To study the effects of the C(2) position, it has commonly been analyzed in its protonated and methylated forms [4,8,19,25–27]. The methylation at C(2) basically removes the possibility to form hydrogen bonds with the anion at this site. The impact of C(2) methylation on the viscosity of imidazolium ionic liquids has been studied extensively, leading to several theories. Fumino's defect theory [7] suggests that the absence of a strong and directional hydrogen bond at C(2) produces a reduced disruption of order. On the other hand, Hunt's reduced entropy theory [28] argues that the methyl group at the C(2) position blocks low energy configurations. Noack et al. [4] showed that electron density changes can alter the position and strength of interionic interactions and lead to reduced configurational variations. Izgorodina's dynamic theory [29] suggests that the free-energy barrier for the anion to move relative to the imidazolium cation increases the viscosity.

The present study aims to shed further light on the role of the C(2) position in imidazolium ionic liquids regarding the interionic interactions with highly symmetrical anions. For this purpose, FTIR, Raman, and H-NMR spectroscopies are applied to the [I^-], [BF_4^-], and [PF_6^-] compounds of 1-methyl-3-propylimidazolium [$MPrIm^+$]. In addition, the thermal behavior is investigated. To study the influence of the hydrogen bonding effects at C(2), the three anions have also been combined with the 1,2-dimethyl-3-propylimidazolium [$MMPrIm^+$] cation. In this cation, the C(2) position is methylated to remove the possibility of acting as a hydrogen bond donor. The chemical structures and the numbering scheme are illustrated in Figure 1. To the best of the authors' knowledge, this work represents the first combined NMR and vibrational spectroscopic study of protonated and methylated imidazolium ILs with systematically varied spherical anions.

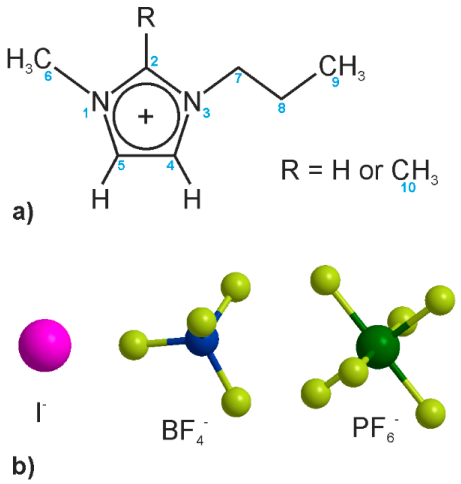

Figure 1. Chemical structure of (**a**) cations and (**b**) anions. The blue numbers in (**a**) indicate the atom numbering used in the discussion.

2. Materials and Methods

2.1. Synthesis and Initial Characterization of Chemicals

The reagents 1-methylimidazole (>99%), 1,2-dimethylimidazole (98%), propyl iodide (98%), ammonium hexafluorophosphate (99.5%), and ammonium tetrafluoroborate (99.5 wt%) were purchased from Fluka and used as received. Deionized H_2O was obtained with a Millipore ion-exchange resin deionizer. MPrImX and MMPrImX (with X = [I^-], [BF_4^-], and [PF_6^-]) were synthesized as follows. A mixture of 1-methylimidazole (7.78 mL, 100 mmol) and propyl iodide (9.74 mL, 50 mmol) was heated at 120 °C for 3 min. During this period, it was additionally exposed to microwaves. The yield of the reaction was 87%. In the next step, the reaction mixture was evaporated at reduced pressure. Then diethyl ether (5 × 20 mL) was used to wash the product several times in order to remove any excess propyl iodide. Thereafter, the product was dried under vacuum for 8 h to remove the solvent, yielding a product with sufficiently high purity. The [BF_4^-] ILs were prepared employing the same procedure. On the other hand, the [PF_6^-] ILs were obtained through a metathesis anion exchange reaction from IL iodide. They were washed with distilled water several times, yielding a 2-phase mixture: the ionic liquid at the bottom and an aqueous solution at the top. The former was separated from the latter by centrifugation (3000 rpm) for 60 s. A rotary evaporator was used to remove residual volatile compounds from the ionic liquid phase at reduced pressure. Then the liquid was washed with fresh ethyl acetate (100 mL).

The same protocols were followed to synthesize the methylated ILs, using 1,2-dimethylimidazole as the precursor. In order to remove water-soluble impurities and obtain sufficiently high purity, all ILs were washed with high-purity water under stirring. Then the 2 phases were separated and dried during continuous agitation under vacuum conditions (≈10 Pa) at 70 °C over several hours to reduce the water content and volatile compounds. Prior to use, all of the ILs were dried on a high-vacuum line ($p < 10^{-5}$ bar) for 4 days at ~40 °C. The water content was measured by coulometric Karl Fischer titration (Metrohm 831). The obtained values are summarized in Table 1. The drying step is important, as the [BF_4^-] and iodide ILs are hydrophilic and significant amounts of water would have an impact on the interionic interactions.

^{1}H NMR (400 MHz), ^{13}C NMR, ^{31}P, and ^{19}F (100.6 MHz) spectra were recorded on a DRX 400 MHz spectrometer. The chemical shifts (δ) are given in ppm and referenced to the internal solvent signals, namely TMS (tetramethylsilane), H_3PO_4, and $CFCl_3$. An initial set of IR spectra for identification purposes was recorded on an FT-IR Perkin-Elmer Spectrum BX spectrophotometer with a resolution of

4 cm^{-1} in the range 4000–650 cm^{-1}. The IR spectra discussed in the Results section were recorded with higher resolution, as described in Section 2.3.

Table 1. Water content of the ionic liquids under investigation.

Ionic Liquid	Abbreviation	Water Content (ppm)
1-Methyl-3-propylimidazolium iodide	$[MPrIm^+][I^-]$	332
1-Methyl-3-propylimidazolium tetrafluoroborate	$[MPrIm^+][BF_4^-]$	48
1-Methyl-3-propylimidazolium hexafluorophosphate	$[MPrIm^+][PF_6^-]$	104
1,2-Dimethyl-3-propylimidazolium iodide	$[MMPrIm^+][I^-]$	307
1,2-Dimethyl-3-propylimidazolium tetrafluoroborate	$[MMPrIm^+][BF_4^-]$	36
1,2-Dimethyl-3-propylimidazolium hexafluorophosphate	$[MMPrIm^+][PF_6^-]$	56

The structures of the obtained products were confirmed using ^1H, ^{13}C, ^{19}F, ^{31}P-NMR, and FT-IR spectroscopy. The data also confirm the absence of significant impurities, e.g., residuals of the reactants or byproducts. The spectroscopic data are given below:

$[MPrIm^+][I^-]$: **^{1}H-NMR** ($CDCl_3$) δ_H (ppm): 9.08 (1H, s, $N_3{}^+C_2\underline{H}N_1$), 7.72 (1H, s, $N_3{}^+C_4\underline{H}$), 7.67 (1H, s, N_1C_5H), 4.11–4.14 (2H, t, J = 4 Hz, $N_3{}^+C_7\underline{H}_2$), 3.86 (3H, s, $N_1C_6\underline{H}_3$), 1.79–1.84 (2H, m, J = 8 Hz, $N_3{}^+C_7H_2C_8\underline{H}_2$), 0.85–0.88 (3H, t, J = 8 Hz, $N_3{}^+C_7H_2C_8H_2C_{10}\underline{H}_3$); **^{13}C-NMR** ($CDCl_3$) δ_C (ppm): 10.4, 23.3, 36.8, 51.1, 122.2, 123.5, 136.0; **IR** ($\tilde{\nu}$/cm^{-1}): 3071 [ν(=C–H)], 2962, 2875 [ν(C–H)], 1567 [ν(C=C)], 1455 [δ(C–H)], 1193 [ν(C–N)], 747 [ν(C–H)].

$[MMPrIm^+][I^-]$: **^{1}H-NMR** ($CDCl_3$) δ_H (ppm): 7.63(1H, s, $N_3{}^+C_4\underline{H}$), 7.60 (1H, s, N_1C_5H), 4.06–4.09 (2H, t, J = 4 Hz, $N_3{}^+C_7\underline{H}_2$), 3.75 (3H, s, $N_1C\underline{H}_3$), 2.58 (3H, s, $N_3{}^+C_2C_{10}\underline{H}_3N$), 1.71–1.77 (2H, m, J = 4 Hz, $N_3{}^+C_7H_2C_8\underline{H}_2$), 0.86–0.89 (3H, t, J = 4 Hz, $N_3{}^+C_7H_2C_8H_2C_9\underline{H}_3$); **^{13}C-NMR** ($CDCl_3$) δ_C (ppm): 10.9, 11.7, 23.2, 36.7, 50.4, 121.3, 122.8, 143.7; **IR** ($\tilde{\nu}$/cm^{-1}): 3074 [ν(=C–H)], 2963, 2876 [ν(C–H)], 1586 [ν(C=C)], 1459, 1419 [δ(C–H)], 1132 [ν(C–N)], 751 [ν(C–H)].

$[MPrIm^+][BF_4^-]$: **^{1}H-NMR** ($CDCl_3$) δ_H (ppm): 9.05 (1H, s, $N_3{}^+C_2\underline{H}N_1$), 7.71 (1H, s, $N_3{}^+C_4\underline{H}$), 7.65 (1H, s, N_1C_5H), 4.10–4.14 (2H, t, J = 4 Hz, $N_3{}^+C_7\underline{H}_2$), 3.85 (3H, s, $N_1C_6\underline{H}_3$), 1.78–1.83 (2H, m, J = 8 Hz, $N_3{}^+C_7H_2C_8\underline{H}_2$), 0.85–0.88 (3H, t, J = 8 Hz, $N_3{}^+C_7H_2C_8H_2C_{10}\underline{H}_3$); **^{19}F-NMR** (DMSO): −148.2 (s, BF_4). **IR** ($\tilde{\nu}$/cm^{-1}): 3077 [ν(=C–H)], 2964, 2877 [ν(C–H)], 1568 [ν(C=C)], 1456 [δ(C–H)], 1167 [ν(C–N)], 1052 [ν(B–F)], 747 [ν(C–H)].

$[MMPrIm^+][BF_4^-]$: **^{1}H-NMR** ($CDCl_3$) δ_H (ppm): 7.33–7.34 (1H, d, $N_3{}^+C_4\underline{H}$), 7.26 (1H, d, N_1C_5H), 3.85–3.89 (2H, t, J = 8 Hz, $N_3{}^+C_7\underline{H}_2$), 3.66 (3H, s, $N_1C\underline{H}_3$), 2.49 (3H, s, $N_3{}^+C_2C_{10}\underline{H}_3N$), 1.48–1.55 (2H, m, J = 4 Hz, $N_3{}^+C_7H_2C_8\underline{H}_2$), 0.62–0.65 (3H, t, J = 4 Hz, $N_3{}^+C_7H_2C_8H_2C_9\underline{H}_3$); IR ν($cm^{-1}$): νCH_3(C–H): 2951, δ(C–H): 1457, ν(C–N): 1273, ν(**B–F**): 1027, ν(C–H): 763; **^{19}F-NMR** (DMSO): –148.2 (s, BF_4). **IR** ($\tilde{\nu}$/cm^{-1}): 3075[ν(=C–H)], 2963,2877[ν(C–H)], 1587[ν(C=C)], 1457 [δ(C–H)], 1241 [ν(C–N)], 1054, 1035 [ν(B–F)], 750 [ν(C–H)].

$[MPrIm^+][PF_6^-]$: **^{1}H-NMR** ($CDCl_3$) δ_H (ppm): 9.21 (1H, s, $N_3{}^+C_2\underline{H}N_1$), 7.82 (1H, s, $N_3{}^+C_4\underline{H}$), 7.75 (1H, s, N_1C_5H), 4.13–4.17 (2H, t, J = 4 Hz, $N_3{}^+C_7\underline{H}_2$), 3.87 (3H, s, $N_1C_6\underline{H}_3$), 1.76–1.82 (2H, m, J = 8 Hz, $N_3{}^+C_7H_2C_8\underline{H}_2$), 0.81–0.85 (3H, t, J = 8 Hz, $N_3{}^+C_7H_2C_8H_2C_{10}\underline{H}_3$); **^{31}P-NMR** (DMSO-d6) δ (ppm): −131, −135.4, −139.8, −144.2, −148.6, −153, −157.4 (septet, $\mathbf{P}F_6^-$); **^{19}F-NMR** (DMSO-d6) δ(ppm): −69.2, −71.1 (d, $P\mathbf{F}_6^-$). **IR** ($\tilde{\nu}$/cm^{-1}): 3168, 3125 [ν(=C–H)], 2973, 2885 [ν(C–H)], 1569 [ν(C=C)], 1462 [δ(C–H)], 1169 [ν(C–N)], 815 [ν(P–F)], 749, 740 [ν(C–H)].

$[MMPrIm^+][PF_6^-]$: **^{1}H-NMR** ($CDCl_3$) δ_H (ppm): 7.31–7.34 (1H, d, $N_3{}^+C_4\underline{H}$), 7.24–7.26 (1H, d, N_1C_5H), 3.84–3.90 (2H, t, J = 4 Hz, $N_3{}^+C_7\underline{H}_2$), 3.67–3.67 (3H, s, $N_1C\underline{H}_3$), 2.48–2.50 (3H, s, $N_3{}^+C_2C_{10}\underline{H}_3N$), 1.51–1.59 (2H, m, J = 4 Hz, $N_3{}^+C_7H_2C_8\underline{H}_2$), 0.63–0.69 (3H, t, J = 4 Hz, $N_3{}^+C_7H_2C_8H_2C_9\underline{H}_3$); **^{31}P-NMR** (DMSO-d6) δ (ppm): −131.1, −135.4, −139.8, −144.2, −148.6, −153, −157.4 (septet, $\mathbf{P}F_6^-$); **^{19}F-NMR** (DMSO-d6) δ(ppm): −69.3, −71.2 (d, PF_6^-). **IR** ($\tilde{\nu}$/cm^{-1}): 3157 [ν(=C–H)], 2974, 2883 [ν(C–H)], 1540 [ν(C=C)], 1462, 1423 [δ(C–H)], 1268 [ν(C–N)], 827 [ν(P–F)], 730, 701 [ν(C–H)].

2.2. Thermal Analysis

Concomitant thermal gravimetric analysis (TGA) and differential scanning calorimetry (DSC) measurements were performed using a Setaram Setsys 1200 instrument under an inert helium flux of 60 mL/min. The temperature ranges from 25 °C to 650 °C was studied with an increment rate of 5 °C/min. According to the manufacturer, the resolution of the DSC is 1 µW and that of the TGA balance is 1 ng, with a potential absolute shift of 100 ng per hour.

2.3. Raman and IR Spectroscopy

The Raman and IR measurements were performed at the Walloon Agricultural Research Center (Craw) Belgium. Fourier transform mid-infrared spectra were acquired on a Bruker Vertex II-70RAM Spectrometer (Bruker Analytical, Madison, WI, USA) operating with a Golden Gate diamond ATR accessory TM (Specac Ltd., Slough, UK). The FTIR spectra (600–3500 cm^{-1}) were collected with 1 cm^{-1} resolution by co-adding 64 scans for each spectrum. FT-Raman spectra were acquired on a Vertex 70-RAM II Bruker FT-Raman spectrometer. This instrument is equipped with an Nd:YAG laser (wavelength 1064 nm, maximum power 1.5 W) and a liquid nitrogen cooled Ge detector. FT-Raman spectra (45–4000 cm^{-1}) were collected with 1 cm^{-1} resolution by co-adding 128 scans for each spectrum at room temperature.

3. Results

3.1. Thermal Behavior

In order to study the effects of methylation at the macroscopic level, the thermal behavior was analyzed using TGA and DSC measurements. The resulting thermograms and heat flux curves are presented in Figure 2. The diagrams on the left display the protonated ILs and those on the right show the behavior of the methylated counterparts. Qualitatively, they appear similar, but the temperatures where phase transitions and thermal decomposition take place vary significantly. The derived numbers are summarized in Table 2. It can be seen that generally, methylation results in an increased melting point. The protonated iodide and tetrafluoroborate ILs are liquid at room temperature, while their methylated counterparts are solid. In the hexafluorophosphate case, both ILs are solid at room temperature, but again, methylation elevates the melting point by 50 K.

Table 2. Thermal properties of C2-methylated and C2-protonated imidazolium-based ionic liquids.

Ionic Liquid	Molecular Weight (g/mol)	Physical State @25 °C	T_m (°C) [1]	T_d (°C) [2]
$[MPrIm^+][I^-]$	252.1	Liquid	– [3]	340
$[MMPrIm^+][I^-]$	266.12	Solid	82	364
$[MPrIm^+][BF_4^-]$	212.11	Liquid	– [3]	338
$[MMPrIm^+][BF_4^-]$	226.02	Solid	62	345
$[MPrIm^+][PF_6^-]$	270.16	Solid	31	486
$[MMPrIm^+][PF_6^-]$	284.18	Solid	81	499

[1] Melting point (onset of the endothermic peak); [2] Decomposition temperature (from thermal gravimetric analysis (TGA) decomposition peak); [3] Not detected in temperature range under study.

Interestingly, methylation at the C(2) position also has an impact on the thermal decomposition. For all three anions, an increased decomposition temperature is observed. This means that the methylation has an impact not only on the thermophysical properties and molecular arrangements, which has previously been shown for other anions [4], but also on the molecular stability. In the following, we make an attempt to understand the molecular phenomena and mechanisms leading to the observed thermal behavior by analyzing the vibrational spectra at room temperature.

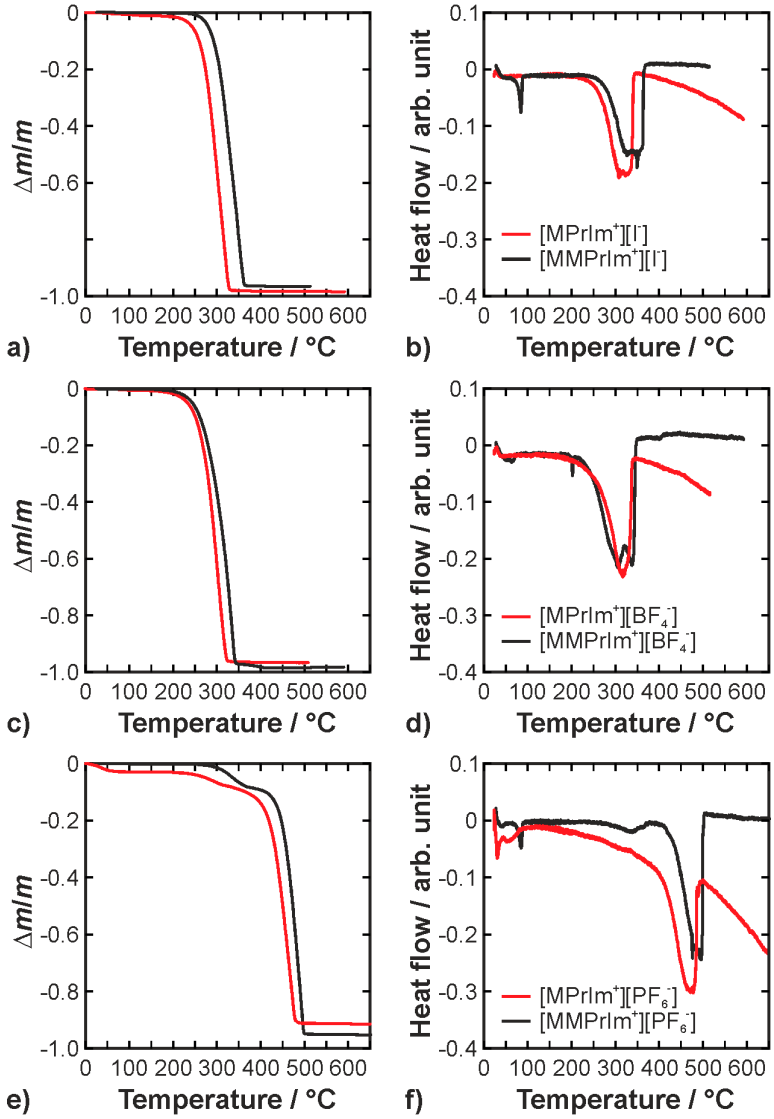

Figure 2. TGA (panels (**a**,**c**,**e**)) and differential scanning calorimetry (DSC) (panels (**b**,**d**,**f**)) curves of the C2-protonated versus C2-methylated imidazolium-based ionic liquids. The legends in the diagrams on the right are also valid for the corresponding diagrams on the left; (**a**) and (**b**) show the data of the iodide ILs; (**c**) and (**d**) show the data of the tetrafluoroborate ILs; (**e**) and (**f**) show the data of the hexafluorophosphate ILs.

3.2. Vibrational Spectra

The full ranges of IR and Raman spectra of all compounds are displayed in Figure 3. The detailed vibrational analysis and tentative assignments are summarized in Tables A1 and A2 in the appendix. The assignments are based on previous work and the references therein [6,19,30]. In the following, we focus on a discussion of the interionic interactions.

The predominant sites of the protonated cation (R = H) for hydrogen bonding interactions are the aromatic CH groups at C(2), C(4), and C(5). As mentioned above, the C(2) proton of imidazolium compounds is slightly acidic, hence it is expected to be the main donor of hydrogen bonds [31]. The formation of a hydrogen bond at C(2) leads to a change in the strength of the covalent C(2)–H bond, which in turn can be observed as a frequency shift of the corresponding vibrational mode. A red shift (i.e., a shift toward lower frequency or wavenumber) means a weakening of the bond, and a blue shift (i.e., a shift toward higher frequency or wavenumber) means strengthening [32].

The formation of strong hydrogen bonds is commonly associated with a red shift. Consequently, the C(2)–H stretching vibration should occur at a lower wavenumber than its C(4)/(5)–H counterparts. This has also been suggested by DFT calculations of other imidazolium-based ionic liquids, e.g., in references [6,16]. The above hypothesis is corroborated by the IR and Raman spectra of the [MPrIm$^+$] ILs in Figure 4a–e. The C(4)/(5)–H stretching vibrations are observed as a single degenerate peak at 3163/3143 (IR/Raman), 3163/3154, and 3171/3181 cm^{-1} for the [I$^-$], [BF$_4^-$], and [PF$_6^-$] compounds, respectively. In contrast, the C(2)–H stretches appear at 2852, 2849, and 3004 cm^{-1}, indicating an involvement in strong hydrogen bonding interactions. For completeness, we note that assignment of the CH stretching bands of imidazolium-based ILs is a subject of ongoing debate (see, for example, [3,22,33–35]) and a definitive conclusion has not yet been reached. The assignment used in the present study is consistent with our previous work; all IL data we have recorded so far point in this direction.

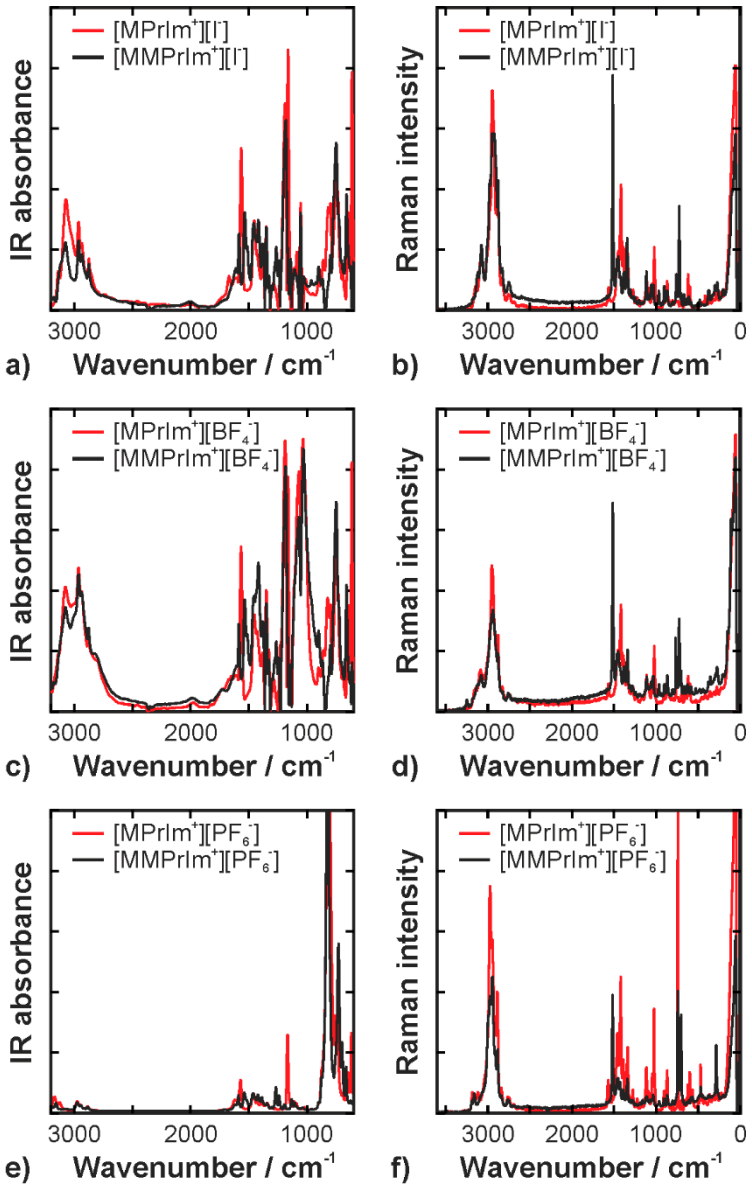

Figure 3. Full range infrared (panels (**a**,**c**,**e**)) and Raman (panels (**b**,**d**,**f**)) spectra; (**a**) and (**b**) show the data of the iodide ILs; (**c**) and (**d**) show the data of the tetrafluoroborate ILs; (**e**) and (**f**) show the data of the hexafluorophosphate ILs.

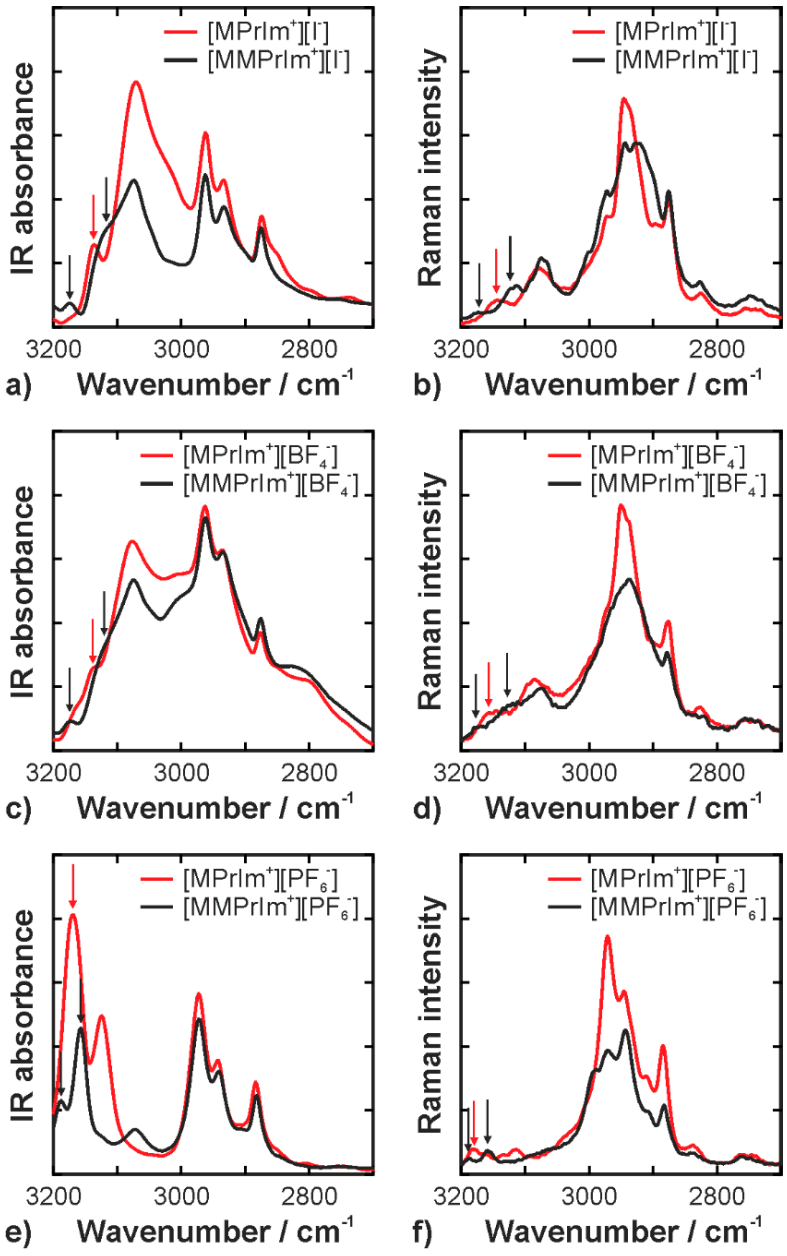

Figure 4. Infrared (**a**,**c**,**e**) and Raman (**b**,**d**,**f**) spectra in the CH stretching region. The relevant peaks and shoulder bands are marked by arrows; (**a**) and (**b**) show the data of the iodide ILs; (**c**) and (**d**) show the data of the tetrafluoroborate ILs; (**e**) and (**f**) show the data of the hexafluorophosphate ILs.

Upon methylation of the C(2) position, the C(2)–H stretching bands disappear and the C(4)/(5)–H are modified in all three types of ionic liquids, suggesting a molecular rearrangement of the anion-cation interactions. Interestingly, the initially degenerate peak of the C(4)/(5)–H stretching modes splits into blue- and red-shifted components. This can be explained by the fact that the anion predominantly interacts with only one of the two protons: a new hydrogen bond is formed at either C(4) or C(5). Consequently, the hydrogen-bonded CH stretch is red-shifted. At the same time, a redistribution of the charge in the aromatic system occurs as a result of the methylation and the hydrogen bond formation. This manifests as a blue shift of the other CH mode. The arrows in Figure 3 mark the initial and resulting bands in the IR and Raman spectra.

The strongest effects are found in the spectra of the [I^-] and [BF_4^-] compounds. In the iodide IL, the IR band at 3136 cm^{-1} is split into a significantly blue-shifted ($\Delta\nu$ = +39 cm^{-1}) and a moderately

red-shifted ($\Delta\nu = -17$ cm^{-1}) peak. On the other hand, for the [BF_4^-] IL, a moderate blue shift ($\Delta\nu = +11$ cm^{-1}) and a significant red shift ($\Delta\nu = -44$ cm^{-1}) are observed. The [PF_6^-] IL places itself in between: blue shift of $\Delta\nu = +17$ cm^{-1} and red shift of $\Delta\nu = -14$ cm^{-1}. This observation perfectly correlates with the polarizability of the three anions: 0.00673 for [I^-] > 0.00418 for [PF_6^-] > 0.00280 for [BF_4^-] according to Bica et al. [36]. This suggests that the anion's polarizability plays an important role in determining not only the strength of the hydrogen bond, but also the charge distribution across the cation. This charge redistribution upon methylation is also reflected by many other vibrational modes of the aromatic ring, e.g., for all three anions, the N–C(6) stretching modes are blue-shifted by about 10 cm^{-1} in the methylated compounds. In summary, the IR and Raman spectra of the C(2) protonated ILs show that the anion interacts with the cation via formation of a strong hydrogen bond at C(2)–H. Upon methylation, the anion moves to the C(4) and C(5) moiety, where it forms a new hydrogen bond with one of the two protons. The spectra do not suggest that other interaction mechanisms, such as those via the π-electron system of the aromatic ring (often referred to as the on-top position [37–39]), play a major role. Moreover, Endo et al. [26] performed an experimental and computational study on methylated and nonmethylated butylimidazolium ILs with spherical anions. They found that the melting points and freezing points of these ILs increase with methylation at the C(2) position. They also found that the Raman bands of [BMIm]I shift red upon C(2) methylation, whereas the bands of [BMIm]BF_4 and [BMIm]PF_6 shift blue. This finding indicates that the anion's position in [BMIm]I is closer to the proton at the 4 or 5 position than in BF_4^- and PF_6^- salts. This is in agreement with our results.

3.3. NMR Spectra

The H-NMR data can shed further light on the effects of C(2) methylation. Table 3 summarizes the measured peaks and their assignments based on [4,40,41]. Signatures of the C(2) and C(10) protons can only be found in the nonmethylated and methylated ILs, respectively. In all three IL pairs, the C(4) and C(5) protons experience an upfield shift upon methylation, which indicates increased electron density. This increase can be explained by the inductive effect of the added methyl group and by charge transfer via the new hydrogen bond. This charge transfer seems to be rather small for iodide, as the upfield shifts are small. Interestingly, the shifts in the protons at the aromatic ring and those in the alkyl side chains are very similar. This indicates that the overall charge distribution at the protons is not significantly altered and almost independent of the position at which the iodide ion interacts with the cation. This is different for the two molecular anions, [BF_4^-] and [PF_6^-]. The NMR spectra show more significant upfield shifts. Moreover, these shifts are stronger for the aromatic protons than for the aliphatic ones. The NMR data suggest that [BF_4^-] and [PF_6^-] transfer more charge to the cation than iodide. This is counterintuitive, as the charge transfer usually decreases with increasing anion size [28,42]: iodide has an ionic radius of 220 pm, while [BF_4^-] and [PF_6^-] exhibit radii of 230 and 245 pm, respectively. Hence, the observed behavior must have another reason. Furthermore, it must be kept in mind that H-NMR provides information about the electron density around the hydrogen atoms. Consequently, the observed shifts do not necessarily allow conclusions to be drawn on the overall interionic charge transfer.

[I^-] can be considered as a sphere, which is geometrically difficult to interact with the cation at multiple sites simultaneously. On the other hand, [BF_4^-] and [PF_6^-] possess several electronegative atoms, which may establish additional Coulomb or dispersion forces with other moieties of the cation, e.g., the alkyl side chains. This situation is shown schematically in Figure 5, taking [I^-] and [BF_4^-] as examples. The [BF_4^-] and [PF_6^-] anions seem large enough to reach the terminal methyl group of the propyl side chain. This would explain why the C(9) protons in the iodide IL show virtually no chemical shift, while significant upfield shifts are observed for [BF_4^-] and [PF_6^-]. However, it must be noted that the molecular arrangement displayed in Figure 5 is not exclusive. In the real liquid, a distribution of several cation/anion configurations will be present simultaneously [43], and the sketch must be seen as one example of what the data suggest exists in larger amounts.

Table 3. ^{1}H-NMR peaks and assignments.

Assignment	[MPrIm$^+$] [I$^-$]	[MMPrIm$^+$] [I$^-$]	[MPrIm$^+$] [BF_4^-]	[MMPrIm$^+$] [BF_4^-]	[MPrIm$^+$] [PF_6^-]	[MMPrIm$^+$] [PF_6^-]
C(2)–H	9.08		9.05		9.21	
C(4)–H	7.72	7.63	7.71	7.33–7.34	7.82	7.31–7.34
C(5)–H	7.67	7.60	7.65	7.26	7.75	7.24–7.26
C(6)–H	3.86	3.75	3.85	3.66	3.87	3.67
C(7)–H	4.11–4.14	4.06–4.09	4.10–4.14	3.85–3.89	4.13–4.17	3.84–3.90
C(8)–H	1.79–1.84	1.71–1.77	1.78–1.83	1.48–1.55	1.76–1.82	1.51–1.59
C(9)–H	0.85–0.88	0.86–0.89	0.85–0.88	0.62–0.65	0.81–0.85	0.63–0.69
C(10)–H		2.58		2.49		2.48–2.50

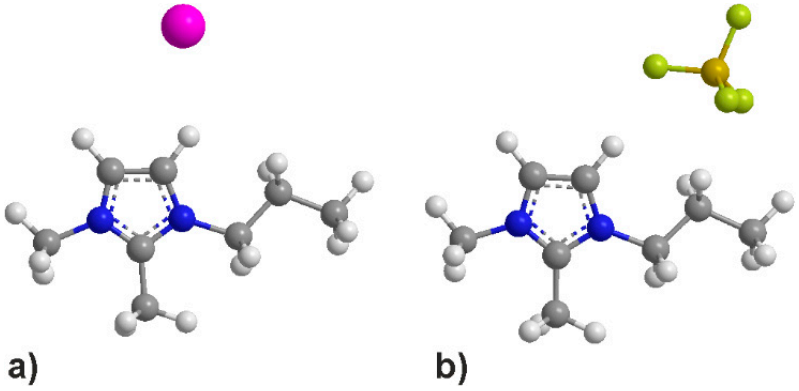

Figure 5. Schematic interaction geometries of (**a**) [MMPrIm$^+$][I$^-$] and (**b**) [MMPrIm$^+$][BF_4^-]. The geometries were energetically optimized using the MM2 function of ChemDraw, but they may not accurately represent the true configuration due to the simplistic underlying model. They are meant to serve as a general illustration of the interaction.

In all three cases, methylation of the C(2) positions results in a replacement of the highly directional interaction between the cation and the anion by a less exclusive one that furthermore allows additional interactions with the ring and the side chains. This is particularly true for the molecular anions, [BF_4^-] and [PF_6^-]. Consequently, the overall molecular system gains symmetry when the C(2) position is methylated. Such an increase in symmetry at the molecular level manifests as altered macroscopic properties. For example, viscosity increases significantly from 35 to 195 cP in the [I$^-$] ILs and from 103 to 330 cP in the [BF_4^-] ILs [29]. The increased symmetry also allows easier formation of a solid crystalline phase, hence an increase in the melting point temperature. For example, in the [PF_6^-] ILs it rises from 40 to 78 °C upon methylation [44]. Similar effects have been observed with a number of other dialkylimidazolium ILs, e.g., NTf_2 and other halogenide anions, and in computational studies [4,5,7,28,29,38]. This suggests that the above findings represent a rather universal phenomenon.

4. Conclusions

In this study, we have investigated the role of the C(2) position in imidazolium-based ionic liquids with highly symmetric anions. A series of compounds in which the C(2) position was either protonated or methylated was analyzed with respect to the thermal and structural (IR, Raman, and H-NMR) properties. In the ILs exhibiting a proton at C(2), this functional group represents the predominant site for interionic interactions via hydrogen bonding. When the proton is replaced by a methyl group, this possibility is removed and the anion rearranges itself at the opposite side of the ring. It forms a new hydrogen bond with either the C(4) or C(5) proton. The split of the initially degenerate C(4)/(5)–H stretching band into red- and blue-shifted new peaks suggests that only one of the two aromatic CH groups is involved in this hydrogen bond. With increased diameter of the anion,

additional interactions seem to take place with the propyl side chain. This is suggested by the NMR spectra. The spectroscopic observations indicate an increase in the homogeneity of the electron distribution upon methylation. This gain in symmetry is reflected at the macroscopic level by an increase in viscosity and melting point. In other words, the methylated ILs are characterized by lower fluid mobility and easier arrangement in a solid crystalline network. Similar behavior has also been found for imidazolium-based ILs with nonsymmetric anions, thus it appears to be a universal phenomenon. A further interesting observation was that methylation of the C(2) position resulted in an increased decomposition temperature. This implies that the changes in the chemical structure and interactions lead to enhanced stability of the compounds. Therefore it may be speculated that the thermal decomposition likely starts at the C(2) moiety. Analyzing the decomposition in more detail would require coupling the TGA with FTIR and mass spectrometry analysis of the flue gas.

Author Contributions: Conceptualization: D.V., H.B., and B.H.; methodology: H.B., S.B., O.A., and A.P.; synthesis: H.B. and D.V.; characterization: S.B., O.A., and O.P.; data analysis: B.H., J.K., O.P., and S.B.; writing–original draft preparation: B.H. and O.P.; writing–review and editing: J.K. and A.P.; supervision: H.B., E.B., and M.R.

Funding: This research received no external funding.

Conflicts of Interest: The authors declare no conflict of interest.

Appendix A

Table A1. Observed FTIR/ATR bands and their tentative assignment of [1-MPrIM+][I^-], [1,2-DMPrIM+][I^-], [1-MPrIM+][BF_4^-], [1,2-DMPrIM+][BF_4^-], [1-MPrIM+][PF_6^-], and [1,2-DMPrIM+][PF_6^-]. vw = very weak, w = weak, m = medium, s = strong, sh = shoulder, Str = stretch, δ = deformation, bend = bending deformation, γ = out of plane deformation, ω = wagging, ρ = rocking, sym = symmetric, asym = asymmetric.

[$MPrIm^+$] [I^-]	[$MMPrIm^+$] [I^-]	[$MPrIm^+$] [BF_4^-]	[$MMPrIm^+$] [BF_4^-]	[$MPrIm^+$] [PF_6^-]	[$MMPrIm^+$] [PF_6^-]	Assignment	References
615 (s)		617 (s)		622 (m)		γ $C_{(2)-H}$/CH_3(N) CN Str	[19,45,46]
			628 (w)			CH_3(N) CN Str	[45,47]
646 (m)		646 (m)		648 (vw)		CH_3(N) CN Str	[19,46]
	663 (m)		663 (m)		667 (w)	ω(C–H)	[19,46]
696 (w)	703 (w)	696 (w)	705 (w)	698 (vw)	700 (w)	CH_2(N)/CH_3(N)CN bend	[19,46]
			727 (sh)		732 (m)	CH_3(N) bend,	[4,20,45]
				740 (w)		ring HCCH sym bend	[4,20,45]
748 (m)	752 (m)	750 (m)	750 (s)	750 (w)		γ C(4,5)–H/H–C–C–H, BF_4 FBF sym str, propyl HCH bend	[19,20,48]
800 (m)	802 (w)	800 (m)	802 (w)			CH_2(N)/, ring HCCH as bend	[46–48]
				815 (s)	825 (s)	FPF asym str, ring HCCH asym bend	[45,49]
			844 (w)			ring HCCH asym bend	[30,47,49]
819 (m)		825 (m)				NC(H)N bend/CCH bend	[46,47]
860 (w)	867 (vw)	860 (w)	865 (vw)	875 (sh)	877 (sh)	asym CH_3(N), ρasym (CH_2)	[45–47]
904 (vw)	900 (vw)	902 (vw)	900 (w)			δasym (H–C–C–H)/CH_3(N)CN/CH_2(N) bend	[19,46]
1020 (sh)		1020 (vw)		1026 (w)		CH_3(N)CN bend	[46]
		1035 (s)	1031 (s)		1039 (w)	BF_4 asym str, CH_3(N)CN bend	[20,49]
1056 (m)	1056 (m)			1051 (vw)		CH_2(N) and CH_3(N)CN Str/CC Str	[4,20,47,48]
1087 (m)		1072 (w)	1072 (m)			CC str, BF_4 asymstr	[20,46]
				1091 (w)	1089 (w)	ring asym str, CH_3(N) bend, ring HCCH sym bend	[30,47,48]
		1110 (w)		1112 (w)	1104 (m)	ring asym str, CH_3(N) bend, ring HCCH sym bend	[20,46,47,49]
	1135 (m)	1137 (w)	1143 (w)		1132 (w)	CC Str,	[20]
1155 (m)						(N)CH_2 and (N)CH_3 CN Str	[20,49]
1164 (s)		1164 (s)		1186 (s)		(N)CH_3CN Str, CH_2(N) and CH_3(N)CN Str/CC Str	[4,19,20,49]
1189 (s)	1186 (s)	1189 (s)	1184 (s)		1193 (w)	CH_2(N) and CH_3(N)CN Str/CC Str	[4,20,49]
		1228 (sh)	1224 (sh)				[46]
	1243 (w)		1243 (w)		1240 (m)	CC Str	[49]
	1267 (m)		1265 (w)		1269 (m)	δ(C–H), CH_3(N)CN Str/CC Str	
		1286 (w)	1282 (sh)			BF_4 FBF asymstr	[20]
			1305 (vw)			ring asym str, CCCH bend, ring HCCH sym bend	[20,49]
1328 (sh)	1328 (sh)	1330 (m)	1330 (vw)			CC str/CH_2(N) str, CH_3(N) CN str	[19,20,47]
				1344 (w)	1344 (w)	CCCH bend, CH_3(N) str, CH_2(N) str	[4,20,49]

Table A1. *Cont.*

[MPrIm$^+$] [I$^-$]	[MMPrIm$^+$] [I$^-$]	[MPrIm$^+$] [BF_4^-]	[MMPrIm$^+$] [BF_4^-]	[MPrIm$^+$] [PF_6^-]	[MMPrIm$^+$] [PF_6^-]	Assignment	References
1351 (m)	1351 (m)	1351 (sh)	1351 (m)			νC–C, CH_2(N),CH_3(N) CN str	[20,49]
1382 (m)	1382 (m)	1384 (m)	1382 (w)	1390 (w)	1388 (w)	δ(CH) δsym (CH_3), CH_2(N),CH_3(N) CN str	[20,49]
	1419		1419 (w)			CH_3(N) CN str	[20,49]
1429 (m)		1429 (m)		1431 (w)	1423 (w)	CH_3(N) CN Str/	[20,49]
						CH_3(N) CN Str, CH_3(N)HCH sym bend	[20,49]
1456 (m)	1456 (m)	1456 (m)	1456 (m)	1461 (m)	1461 (w)	CCH HCH asym bend, CH_3(N)HCH sym bend, terminal CH_3 HCH asym bend	[20,49]
			1513 (sh)		1515 (sh)	ring asym str, CH_3(N) HCH bend	[20,49]
			1537 (w)		1539 (m)	CCC all HCH sym bend	[20,49]
1567 (m)	1567 (m)	1567 (s)		1571 (m)		asym str CH_2(N)/CH_3(N)CN str/νC=C	[49]
			1587 (m)		1591 (m)	ring asym str, CH_3(N) str, CH_2(N) str	[4,20,49,50]
1610 (vw)						ring asym str, (N)CH_2 and (N)CH_3 CN str	[20,49]
				1620 (sh)	1618 (sh)		[20,49]
	1674 (w)	1672 (vw)				ring C=C Str, CH_3(N)CN Str	[20,46,49]
2875 (w)	2875 (w)	2877 (w)	2875 (w)			propyl C–H νssCH_2	[19,50,51]
				2883 (w)	2883 (w)	CH_3 (sym), propyl C–H	[4,40,52]
2933 (w)	2933 (w)	2935 (w)	2931 (w)			propyl C–H	[4,19,40,50–52]
				2943 (w)	2943 (w)	(N)CH_3	[3,4,19,40,48,50–53]
2962 (w)	2962 (w)	2962 (w)	2962 (w)			propyl CH_3	[3,4,19,40,48,50–53]
				2973 (m)	2972 (m)	N–CH_3 (sym)	[3,4,19,40,48,50–53]
3071 (m)	3071 (m)	3070 (m)	3074 (m)			N–CH_3 (asym)	[3,4,19,40,48,50–53]
	3119 (w)		3119 (w)		3157 (w)	C(4,5)–H	[3,4,19,30,40,48,50–53]
3136 (w)		3163 (w)		3171 (w)		C(4,5)–H	[3,4,19,30,40,48,50–53]
	3175 (w)		3174 (w)		3188 (w)	C(4,5)–H	[3,4,19,30,40,48,50–53]

Table A2. Observed FT-Raman bands and their tentative assignment of [1-MPrIM+][I^-], [1,2-DMPrIM+][I^-], [1-MPrIM+][BF_4^-], [1,2-DMPrIM+][BF_4^-], [1-MPrIM+][PF_6^-], and [1,2-DMPrIM+][PF_6^-]. vw = very weak, w = weak, m = medium, s = strong, sh = shoulder, Str = stretch, δ = deformation, bend = bending deformation, γ = out of plane deformation, ω = wagging, ρ = rocking, sym = symmetric, asym = asymmetric.

[MPrIm$^+$] [I^-]	[MMPrIm$^+$] [I^-]	[MPrIm$^+$] [BF_4^-]	[MMPrIm$^+$] [BF_4^-]	[MPrIm$^+$] [PF_6^-]	[MMPrIm$^+$] [PF_6^-]	Assignment	References
	204 (vw)		203 (w)		205 (vw)	γN–CH_3	[48]
227 (vw)		229 (w)		227 (w)		γN–CH_3/CH_3(N) bend, CH_2(N) bend	[20,49]
279 (vw)	272 (vw)	281 (w)	274 (m)	279 (w)	287 (w)	CH_3(N) and CH_2(N) CN bend	[20,49]
	300 (vw)					CH_2(N), CH_3(N)CH bend	[4,20,45,47,49,50]
		313 (w)		312 (w)			[20,45–47]
365 (vw)		357 (w)	356 (w)			δNCH_3	[20,49,50]
	377 (vw)		375 (w)	363 (w)		CH_3(N) and CH_2(N) CN bend, CCC bend	[20,49]
		400 (vw)					[45,49]
417 (vw)		417 (w)	423 (w)	419 (w)		CH_2(N), CH_3(N)CH bend	[20,49]
			440 (w)				[20,49]
		455 (w)					[20,49]
	481 (vw)		478 (w)	471 (m)	472 (w)		[49]
		527 (vw)	528 (w)			BF_4 scissors	[20,50]
					568 (w)	FPF sym bend	[45,49]
			583 (w)				[50]
600 (w)	609 (vw)	603 (m)	609 (w)	600 (m)		CH_2(N) Str, CH_3(N)CN Str	[4,47,50]
619 (m)		620 (m)		623 (w)		γ $C_{(2)-H}$/CH_3(N) CN Str	[19,46,50]
	630 (vw)		628 (w)			ν(N_C)/CH_2(N), CH_3(N) CN Str	[19,46,50]
		645 (vw)				CH_2(N) and CH_3(N) CN Str	[19]
659 (vw)	667 (vw)	662 (vw)	666 (w)	661 (w)		CH_2(N) Str, CH_3(N)CN Str/ν N–CH_3	[46]
696 (vw)	704 (vw)	696 (w)	703 (w)			CH_2(N)/CH_3(N)CN Str	[19,46,50]
	724 (m)		725 (s)		724 (m)	ring HCCH sym bend, CH_2(N) and CH_3(N) CN	[4,19,46,50]
				742 (s)	742 (m)	ring HCCH asym bend, CH_3(N) Str, CH_2(N) Str	[3,4,19,46,50]
		763 (w)					[3,19,46,50]
	760 (w)	767 (m)	769 (s)			ring HCCH asym bend/ω(CH_2) rocking	[19,46,50]
			783 (sh)				[19,46,50]
			802 (w)	801 (w)	802 (vw)	FPF asym str, ring HCCH asym bend	[45,46,49]
		841 (w)					[47,49,50]
868 (vw)	866 (vw)	868 (m)	866 (m)	867 (w)	876 (vw)	NC(H)N/propyl chain CCC sym str	[19,46,50]
	880 (vw)					propyl chain CCC sym str	[19,46,50]
904 (vw)	903 (vw)	906 (w)	902 (m)	905 (w)	901 (vw)	CCC str	[19,46,50]
			932 (w)				[19,46,50]
	967 (vw)		964 (m)		966 (vw)	ring HCCH sym bend, CH_2(N) and CH_3(N) CN	[19,46,50]
				1014 (sh)		CH_2(N) and CH_3(N) CN str	[19,46,50]

Table A2. *Cont.*

[MPrIm$^+$] [I$^-$]	[MMPrIm$^+$] [I$^-$]	[MPrIm$^+$] [BF_4^-]	[MMPrIm$^+$] [BF_4^-]	[MPrIm$^+$] [PF_6^-]	[MMPrIm$^+$] [PF_6^-]	Assignment	References
1021 (m)		1021 (m)		1024 (m)		ν(C-C)/CH_2(N)/CH_3(N)CN Str, BF_4 asym str	[19,46,50]
1043 (vw)	1033 (vw)	1043 (w)	1034 (w)	1041 (w)	1034 (vw)	CH_2(N) Str, CH_3(N)CN Str	[19,46,50]
	1058 (vw)		1054 (w)			νasym(chain CCC), NCH_3 twist,	[19,46,50]
			1076 (vw)			CH_3(N) CH bend, ring CN asym str	[19,46,50]
		1089 (sh)		1092 (w)		CH_3(N) CH bend, ring CN asym str	[19,46,50]
1113 (w)	1114 (w)	1113 (m)	1113 (w)	1115 (m)	1114 (vw)	CCC str/δ C–H	[19,46,50]
					1160 (vw)	CH_3(N) bend	[19,46,50]
		1186 (vw)		1174 (w)		ring asym str, CH_3(N) Str, CH_2(N) Str	[19,46,50]
1225 (vw)		1224 (w)		1226 (vw)		CC Str	[20,49]
1271 (vw)		1271 (vw)		1275 (w)		δCH	[20,49]
		1284 (sh)	1281 (vw)				[20,49]
	1303 (vw)		1306 (vw)			ρ(C–H)/CN ring	[20,49]
		1313 (vw)				CH_2(N)/CH_3(N)CN Str	[20,49]
1337 (w)	1342 (w)	1337 (m)	1339 (m)	1337 (m)	1339 (vw)	CH_2(N)/CH_3(N)CN Str	[20,49]
1386 (w)	1378 (vw)	1387 (w)	1381 (w)	1389 (w)	1388 (w)	δsCH_3/νas(C(2)N(1)C(5))	[20,49]
1416 (m)		1417 (s)		1419 (m)	1427 (w)	δsCH_3/CH_2(N)/CH_3(N)CN Str, δ(CH_2)	[20,30,49]
1446 (w)	1446 (w)	1445 (sh)	1445 (w)			νC–C, νCH_3–N–CN	[20,49]
		1452 (w)	1459 (w)	1457 (m)	1450 (w)	δCH_3/CH_3(N)HCH sym bend	[20,49]
						(N)CH_3 HCH sym bend, (N)CH_3 CN Str	[20,49]
	1515 (s)		1515 (s)		1516 (m)	NC(CH3)N CC Str, ring CH_3 HCH asym bend	[20,49]
1564 (vw)		1565 (m)		1569 (w)		NC(H)N, ν(R)-MIm$^+$/CH_2(N) Str, CH_3(N)CN Str	[20,49]
2756 (vw)	2749 (w)					propyl C–H	
2825 (vw)	2826 (vw)	2825 (vw)	2822 (vw)	2839 (vw)	2835 (vw)	propyl C–H	[19,51]
2876 (w)	2876 (w)	2876 (w)	2877 (vw)	2884 (vw)	2882 (vw)	νsymCH_3/propyl C–H	[40,51,52]
			2903 (sh)	2903 (sh)	2908 (sh)		[3,19,40,51,52]
2927 (w)		2927 (sh)	2935 (w)			νFRCH_3/ν_{as}(CH_2)/propyl C–H	[3,19,40,51–53]
2945 (m)	2944 (w)	2950 (m)		2945 (sh)	2942 (sh)	ν_s(CH_3)/propyl C–H	[3,4,19,40,51,52]
2973 (sh)	2972 (sh)			2970 (m)	2972 (m)	νasymCH_3	[3,4,19,40,51,52]
					2991 (sh)	FR N–CH_3	[3,4,19,40,51–53]
3076 (w)	3074 (w)	3085 (w)	3074 (w)			νC(2)–H,νC(4,5)–H	[3,4,19,40,48,50–53]
				3114 (vw)			[3,4,19,40,48,50–53]
		3146 (w)		3134 (vw)		νC(2)–H	[3,4,19,30,40,48,50–53]
				3160 (vw)	3159 (vw)	C(4,5)–H	[3,4,19,30,40,48,50–53]
				3183 (vw)	3187 (vw)	C(4,5)–H	[3,4,19,30,40,48,50–53]
			3246 (w)			C(4,5)–H	[3,4,19,30,40,48,50–53]

References

1. Armand, M.; Endres, F.; MacFarlane, D.R.; Ohno, H.; Scrosati, B. Ionic-liquid materials for the electrochemical challenges of the future. *Nat. Mater.* **2009**, *8*, 621–629. [CrossRef] [PubMed]
2. Werner, S.; Haumann, M.; Wasserscheid, P. Ionic liquids in chemical engineering. *Ann. Rev. Chem. Biomol. Eng.* **2010**, *1*, 203–230. [CrossRef] [PubMed]
3. Paschoal, V.H.; Faria, L.F.O.; Ribeiro, M.C.C. Vibrational Spectroscopy of Ionic Liquids. *Chem. Rev.* **2017**, *117*, 7053–7112. [CrossRef] [PubMed]
4. Noack, K.; Schulz, P.S.; Paape, N.; Kiefer, J.; Wasserscheid, P.; Leipertz, A. The role of the C2 position in interionic interactions of imidazolium based ionic liquids: A vibrational and NMR spectroscopic study. *Phys. Chem. Chem. Phys.* **2010**, *12*, 14153–14161. [CrossRef] [PubMed]
5. Fumino, K.; Wulf, A.; Ludwig, R. The cation-anion interaction in ionic liquids probed by far-infrared spectroscopy. *Angew. Chem. Int. Ed.* **2008**, *47*, 3830–3834. [CrossRef] [PubMed]
6. Dhumal, N.R.; Noack, K.; Kiefer, J.; Kim, H.J. Molecular structure and interactions in the ionic liquid 1-ethyl-3-methylimidazolium bis(trifluoromethylsulfonyl)Imide. *J. Phys. Chem. A* **2014**, *118*, 2547–2557. [CrossRef] [PubMed]
7. Fumino, K.; Wulf, A.; Ludwig, R. Strong, localized, and directional hydrogen bonds fluidize ionic liquids. *Angew. Chem. Int. Ed.* **2008**, *47*, 8731–8734. [CrossRef] [PubMed]
8. Fumino, K.; Wulf, A.; Ludwig, R. The Potential Role of Hydrogen Bonding in Aprotic and Protic Ionic Liquids. *Phys. Chem. Chem. Phys.* **2009**, *11*, 8790–8794. [CrossRef] [PubMed]
9. Dhumal, N.R.; Kim, H.J.; Kiefer, J. Electronic structure and normal vibrations of the 1-ethyl-3-methylimidazolium ethyl sulfate ion pair. *J. Phys. Chem. A* **2011**, *115*, 3551–3558. [CrossRef] [PubMed]
10. Kiefer, J.; Noack, K.; Penna, T.C.; Ribeiro, M.C.C.; Weber, H.; Kirchner, B. Vibrational signatures of anionic cyano groups in imidazolium ionic liquids. *Vib. Spectrosc.* **2017**, *91*, 141–146. [CrossRef]
11. Dhumal, N.R.; Kim, H.J.; Kiefer, J. Molecular interactions in 1-ethyl-3-methylimidazolium acetate ion pair: A density functional study. *J. Phys. Chem. A* **2009**, *113*, 10397–10404. [CrossRef] [PubMed]
12. Bharadwaj, V.S.; Schutt, T.C.; Ashurst, T.C.; Maupin, C.M. Elucidating the conformational energetics of glucose and cellobiose in ionic liquids. *Phys. Chem. Chem. Phys.* **2015**, *17*, 10668–10678. [CrossRef] [PubMed]
13. Kiefer, J.; Pye, C.C. Structure of the room-temperature ionic liquid 1-hexyl-3-methylimidazolium hydrogen sulfate: Conformational isomerism. *J. Phys. Chem. A* **2010**, *114*, 6713–6720. [CrossRef] [PubMed]
14. Ribeiro, M.C.C. High Viscosity of Imidazolium Ionic Liquids with the Hydrogen Sulfate Anion: A Raman Spectroscopy Study. *J. Phys. Chem. B* **2012**, *116*, 7281–7290. [CrossRef] [PubMed]
15. Giraud, G.; Gordon, C.M.; Dunkin, I.R.; Wynne, K. The effects of anion and cation substitution on the ultrafast solvent dynamics of ionic liquids: A time-resolved optical Kerr-effect spectroscopic study. *J. Chem. Phys.* **2003**, *119*, 464–477. [CrossRef]
16. Singh, D.K.; Rathke, B.; Kiefer, J.; Materny, A. Molecular Structure and Interactions in the Ionic Liquid 1-Ethyl-3-methylimidazolium Trifluoromethanesulfonate. *J. Phys. Chem. A* **2016**, *120*, 6274–6286. [CrossRef] [PubMed]
17. Hunt, P.A.; Kirchner, B.; Welton, T. Characterising the electronic structure of ionic liquids: An examination of the 1-butyl-3-methylimidazolium chloride ion pair. *Chem. Eur. J.* **2006**, *12*, 6762–6775. [CrossRef] [PubMed]
18. Skarmoutsos, I.; Dellis, D.; Matthews, R.P.; Welton, T.; Hunt, P.A. Hydrogen bonding in 1-butyl- and 1-ethyl-3-methylimidazolium chloride ionic liquids. *J. Phys. Chem. B* **2012**, *116*, 4921–4933. [CrossRef] [PubMed]
19. Haddad, B.; Mokhtar, D.; Goussem, M.; Belarbi, E.H.; Villemin, D.; Bresson, S.; Rahmouni, M.; Dhumal, N.R.; Kim, H.J.; Kiefer, J. Influence of methyl and propyl groups on the vibrational spectra of two imidazolium ionic liquids and their non-ionic precursors. *J. Mol. Struct.* **2017**, *1134*, 582–590. [CrossRef]
20. Heimer, N.E.; Del Sesto, R.E.; Meng, Z.; Wilkes, J.S.; Carper, W.R. Vibrational spectra of imidazolium tetrafluoroborate ionic liquids. *J. Mol. Liq.* **2006**, *124*, 84–95. [CrossRef]
21. Tsuzuki, S.; Tokuda, H.; Mikami, N. Theoretical analysis of the hydrogen bond of imidazolium C2-H with anions. *Phys. Chem. Chem. Phys.* **2007**, *9*, 4780–4784. [CrossRef] [PubMed]
22. Grondin, J.; Lassègues, J.C.; Cavagnat, D.; Buffeteau, T.; Johansson, P.; Holomb, R. Revisited vibrational assignment of imidazolium-based ionic liquids. *J. Raman Spectrosc.* **2011**, *42*, 733–743. [CrossRef]

23. Dong, K.; Zhang, S.; Wang, D.; Yao, X. Hydrogen bonds in imidazolium ionic liquids. *J. Phys. Chem. A* **2006**, *110*, 9775–9782. [CrossRef] [PubMed]
24. Hamaguchi, H.; Saha, S.; Ozawa, R.; Hayashi, S. Raman and X-ray studies on the structure of [bmim]X (X = Cl, Br, I, [BF4], [PF6]): Rotational isomerism of the [bmim](+) cation. In *Ionic Liquids IIIA: Fundamentals, Progress, Challenges, and Opportunities, Properties and Structure*; Rogers, R.D., Seddon, K.R., Eds.; American Chemical Society: Washington, DC, USA, 2005; Volume 901, pp. 68–78.
25. Namboodiri, M.; Kazemi, M.M.; Khan, T.Z.; Materny, A.; Kiefer, J. Ultrafast vibrational dynamics and energy transfer in imidazolium ionic liquids. *J. Am. Chem. Soc.* **2014**, *136*, 6136–6141. [CrossRef] [PubMed]
26. Endo, T.; Kato, T.; Nishikawa, K. Effects of Methylation at the 2 Position of the Cation Ring on Phase Behaviors and Conformational Structures of Imidazolium-Based Ionic Liquids. *J. Phys. Chem. B* **2010**, *114*, 9201–9208. [CrossRef] [PubMed]
27. Rodrigues, A.S.M.C.; Lima, C.F.R.A.C.; Coutinho, J.A.P.; Santos, L.M.N.B.F. Nature of the C2-methylation effect on the properties of imidazolium ionic liquids. *Phys. Chem. Chem. Phys.* **2017**, *19*, 5326–5332. [CrossRef] [PubMed]
28. Hunt, P.A.; Gould, I.R.; Kirchner, B. The structure of imidazolium-based ionic liquids: Insights from ion-pair interactions. *Aust. J. Chem.* **2007**, *60*, 9–14. [CrossRef]
29. Izgorodina, E.I.; Maganti, R.; Armel, V.; Dean, P.M.; Pringle, J.M.; Seddon, K.R.; MacFarlane, D.R. Understanding the effect of the C2 proton in promoting low viscosities and high conductivities in imidazolium-based ionic liquids: Part I. weakly coordinating anions. *J. Phys. Chem. B* **2011**, *115*, 14688–14697. [CrossRef] [PubMed]
30. Kiefer, J.; Fries, J.; Leipertz, A. Experimental vibrational study of imidazolium-based ionic liquids: Raman and infrared spectra of 1-ethyl-3-methylimidazolium bis(trifluoromethylsulfonyl)imide and 1-ethyl-3-methylimidazolium ethylsulfate. *Appl. Spectrosc.* **2007**, *61*, 1306–1311. [CrossRef] [PubMed]
31. Haake, P.; Bausher, L.P.; McNeal, J.P. Fundamental studies on models for thiamine. Generation of ylides of oxazolium, imidazolium, and thiazolium ions by decarboxylation. Applications to the structure of the thiamine ylide. *J. Am. Chem. Soc.* **1971**, *93*, 7045–7049. [CrossRef] [PubMed]
32. Joseph, J.; Jemmis, E.D. Red-, blue-, or no-shift in hydrogen bonds: A unified explanation. *J. Am. Chem. Soc.* **2007**, *129*, 4620–4632. [CrossRef] [PubMed]
33. Lassègues, J.C.; Grondin, J.; Cavagnat, D.; Johansson, P. New interpretation of the CH stretching vibrations in imidazoliu-based ionic liquids. *J. Phys. Chem. A* **2009**, *113*, 6419–6421. [CrossRef] [PubMed]
34. Lassègues, J.C.; Grondin, J.; Cavagnat, D.; Johansson, P. Reply to the "Comment on 'New interpretation of the CH stretching vibrations in imidazolium-based ionid liquids'". *J. Phys. Chem. A* **2010**, *114*, 687–688. [CrossRef]
35. Wulf, A.; Fumino, K.; Ludwig, R. Comment on "New interpretation of the CH stretching vibrations in imidazolium-based ionid liquids.". *J. Phys. Chem. A* **2010**, *114*, 685–686. [CrossRef] [PubMed]
36. Bica, K.; Deetlefs, M.; Schröder, C.; Seddon, K.R. Polarisabilities of alkylimidazolium ionic liquids. *Phys. Chem. Chem. Phys.* **2013**, *15*, 2703–2711. [CrossRef] [PubMed]
37. Kempter, V.; Kirchner, B. The role of hydrogen atoms in interactions involving imidazolium based ionic liquids. *J. Mol. Struct.* **2010**, *972*, 22–34. [CrossRef]
38. Lehmann, S.B.C.; Roatsch, M.; Schöppke, M.; Kirchner, B. On the physical origin of the cation-anion intermediate bond in ionic liquids Part I. Placing a (weak) hydrogen bond between two charges. *Phys. Chem. Chem. Phys.* **2010**, *12*, 7473–7486. [CrossRef] [PubMed]
39. Kiefer, J.; Molina Martinez, M.; Noack, K. The peculiar nature of molecular interactions between an imidazolium ionic liquid and acetone. *ChemPhysChem* **2012**, *13*, 1213–1220. [CrossRef] [PubMed]
40. Cha, S.; Ao, M.; Sung, W.; Moon, B.; Ahlström, B.; Johansson, P.; Ouchi, Y.; Kim, D. Structures of ionic liquid-water mixtures investigated by IR and NMR spectroscopy. *Phys. Chem. Chem. Phys.* **2014**, *16*, 9591–9601. [CrossRef] [PubMed]
41. Wulf, A.; Fumino, K.; Michalik, D.; Ludwig, R. IR and NMR properties of ionic liquids: Do they tell us the same thing? *ChemPhysChem* **2007**, *8*, 2265–2269. [CrossRef] [PubMed]
42. Rigby, J.; Izgorodina, E.I. Assessment of atomic partial charge schemes for polarisation and charge transfer effects in ionic liquids. *Phys. Chem. Chem. Phys.* **2013**, *15*, 1632–1646. [CrossRef] [PubMed]

43. Vyas, S.; Dreyer, C.; Slingsby, J.; Bicknase, D.; Porter, J.M.; Maupin, C.M. Electronic Structure and Spectroscopic Analysis of 1-Ethyl-3-methylimidazolium Bis(trifluoromethylsulfonyl)imide Ion Pair. *J. Phys. Chem. A* **2014**, *118*, 6873–6882. [CrossRef] [PubMed]
44. Ngo, H.L.; LeCompte, K.; Hargens, L.; McEwen, A.B. Thermal properties of imidazolium ionic liquids. *Thermochim. Acta* **2000**, *357*, 97–102. [CrossRef]
45. Moumene, T.; Belarbi, E.H.; Haddad, B.; Villemin, D.; Abbas, O.; Khelifa, B.; Bresson, S. Vibrational spectroscopic study of imidazolium dicationic ionic liquids: Effect of alkyl chain length. *J. Appl. Spectrosc.* **2016**, *83*, 165–171. [CrossRef]
46. Kadari, M.; Belarbi, E.H.; Moumene, T.; Bresson, S.; Haddad, B.; Abbas, O.; Khelifa, B. Comparative study between 1-propyl-3-methylimidazolium bromide and trimethylene bismethylimidazolium brimode ionic liquids by FTIR/ATR and FT-Raman spectroscopies. *J. Mol. Struct.* **2017**, *1143*, 91–99. [CrossRef]
47. Moumene, T.; Belarbi, E.H.; Haddad, B.; Villemin, D.; Abbas, O.; Khelifa, B.; Bresson, S. Vibrational spectroscopic study of ionic liquids: Comparison between monocationic and dicationic imidazolium ionic liquids. *J. Mol. Struct.* **2014**, *1065*, 86–92. [CrossRef]
48. Moschovi, A.M.; Ntais, S.; Dracopoulos, V.; Nikolakis, V. Vibrational spectroscopic study of the protic ionic liquid 1-H-3-methylimidazolium bis(trifluoromethanesulfonyl)imide. *Vib. Spectrosc.* **2012**, *63*, 350–359. [CrossRef]
49. Talaty, E.R.; Raja, S.; Storhaug, V.J.; Dölle, A.; Carper, W.R. Raman and infrared spectra and ab initio calculations of C_{2-4}MIM imidazolium hexafluorophosphate ionic liquids. *J. Phys. Chem. B* **2004**, *108*, 13177–13184. [CrossRef]
50. Katsyuba, S.A.; Dyson, P.J.; Vandyukova, E.E.; Chernova, A.V.; Vidiš, A. Molecular structure, vibrational spectra, and hydrogen bonding of the ionic liquid 1-ethyl-3-methyl-1*H*-imidazlium tetrafluoroborate. *Helv. Chim. Acta* **2004**, *87*, 2556–2565. [CrossRef]
51. Rivera-Rubero, S.; Baldelli, S. Surface characterization of 1-butyl-3methylimidazolium Br-, I-, PF_6-, BF_4-, $(CF_3SO_2)_2N$-, SCN-, CH_3SO3-, CH_3SO_4-, and $(CN)_2N$- ionic liquids by sum frequency generation. *J. Phys. Chem. B* **2006**, *110*, 4756–4765. [CrossRef] [PubMed]
52. Gao, Y.; Zhang, L.; Wang, Y.; Li, H. Probing electron density of H-bonding between cation-anion of imidazolium-based ionic liquids with different anions by vibrational spectroscopy. *J. Phys. Chem. B* **2010**, *114*, 2828–2833. [CrossRef] [PubMed]
53. Booth, R.S.; Annesley, C.J.; Young, J.W.; Vogelhuber, K.M.; Boatz, J.A.; Stearns, J.A. Identification of multiple conformers of the ionic liquid [emim][tf2n] in the gas phase using IR/UV action spectroscopy. *Phys. Chem. Chem. Phys.* **2016**, *18*, 17037–17043. [CrossRef] [PubMed]